Morphological comparison of the craniofacial phenotypes of mouse models expressing the Apert FGFR2 S252W mutation in neural crest- or mesoderm-derived tissues

Yann Heuzé, Nandini Singh, Claudio Basilico, Ethylin Wang Jabs, Greg Holmes, Joan Richtsmeier

Published in final edited form as:
Bone. 2014 June ; 63: 101–109. doi:10.1016/j.bone.2014.03.003.

Morphological comparison of the craniofacial phenotypes of mouse models expressing the Apert FGFR2 S252W mutation in neural crest- or mesoderm-derived tissues

Yann Heuzé[a], **Nandini Singh**[a], **Claudio Basilico**[b], **Ethylin Wang Jabs**[c], **Greg Holmes**[c], and **Joan T Richtsmeier**[a,*]

[a]Department of Anthropology, Pennsylvania State University, University Park, PA, USA

[b]Department of Microbiology, New York University School of Medicine, New York, NY, USA

[c]Department of Genetics and Genomic Sciences, Mount Sinai School of Medicine, New York, NY, USA

Abstract

Bones of the craniofacial skeleton are derived from two distinct cell lineages, cranial neural crest and mesoderm, and articulate at sutures and synchondroses which represent major bone growth sites. Premature fusion of cranial suture(s) is associated with craniofacial dysmorphogenesis caused in part by alteration in the growth potential at sutures and can occur as an isolated birth defect or as part of a syndrome, such as Apert syndrome. Conditional expression of the Apert FGFR2 S252W mutation in mesoderm was previously shown to be necessary and sufficient to cause coronal craniosynostosis. Here we used micro computed tomography images of mice expressing the Apert mutation constitutively in either mesoderm or neural crest to quantify craniofacial shape variation and suture fusion patterns, and to identify shape changes in craniofacial bones derived from the lineage not expressing the mutation, referred to here as secondary shape changes. Our results show that at postnatal day 0: (i) conditional expression of the FGFR2 S252W mutation in neural crest-derived tissues causes a more severe craniofacial phenotype than when expressed in mesoderm-derived tissues; and (ii) both mesoderm- and neural crest-specific mouse models display secondary shape changes. We also show that premature suture fusion is not necessarily dependent on the expression of the FGFR2 S252W mutation in the sutural mesenchyme. More specifically, it appears that suture fusion patterns in both mouse models are suture-specific resulting from a complex combination of the influence of primary abnormalities of biogenesis or signaling within the sutures, and timing.

*Corresponding author: Joan T Richtsmeier; Department of Anthropology, Pennsylvania State University, Carpenter Building, University Park, PA 16802; Tel: +1 814 863 0562; jtr505@gmail.com.

Keywords

Apert syndrome; FGFR2; Neural Crest; Mesoderm; Suture fusion pattern; Craniosynostosis

1 Introduction

The craniofacial skeleton is comprised of bones that are derived from two distinct cell lineages: cranial neural crest and mesoderm. Cranial neural crest give rise to the facial skeleton, the anterior elements of the cranial base and the frontal bones, while mesoderm produces the components of the occipital, the parietal bones and the non-squamous part of the temporal bones [1–3]. It has been shown in mice that the interparietal is derived from both mesoderm (lateral parts) and neural crest (central part) [1–3]. The different bones of the skull articulate at sutures and synchondroses, which represent major bone growth sites [4]. The premature fusion of one or several calvarial sutures (craniosynostosis) is associated with craniofacial dysmorphogenesis caused in part by altered growth potential at sutures and can occur as an isolated anomaly or as part of a syndrome. Activating mutations in fibroblast growth factor receptor 2 (FGFR2) are causative for some of the craniosynostosis syndromes [5] such as Apert syndrome [OMIM 101200] that is characterized by craniosynostosis and syndactyly of hands and feet, and can include additional cranial and postcranial anomalies [6]. Apert syndrome birth prevalence is about 15.5 in 1,000,000 newborns [7]. Almost 99% of Apert syndrome cases are caused by one of two FGFR2 mutations [8], S252W and P253R, which reside on neighboring amino acids in the linker region between the second and third extra-cellular immunoglobulin domains. These two gain-of-function mutations alter the ligand-binding affinity and specificity of the receptors causing changes in FGFR2 signaling [8]. The craniofacial phenotype of Apert syndrome includes bicoronal craniosynostosis, brachycephaly of the cranial vault, and midfacial dysmorphogenesis. The associated midfacial deformity, often called midfacial hypoplasia or retrusion [9], is a complex trait that is among the most challenging clinical concerns of the FGFR-related craniosynostosis syndromes, affecting oral health, feeding and airway function [5,10].

Using mesoderm- and neural crest-specific Cre drivers [11,12] in combination with the Cre-inducible *Fgfr2*^{S252W} mutant allele [13,14] and *β-galactosidase* [15], Holmes and Basilico [16] showed that the mesodermal expression of the FGFR2 S252W mutation is necessary and sufficient to induce craniosynostosis of the coronal suture. The expression of the FGFR2 S252W mutation induces the mesoderm-derived mesenchyme of the coronal suture to undergo abnormal osteogenesis. The integrity of the lineage border between neural crest and mesoderm is maintained in mutants expressing the *Fgfr2*^{S252W} allele in neural crest and in mutants expressing the mutant allele in mesoderm [16]. Consequently, premature fusion of the coronal suture observed in the mesoderm mutants is not associated with the loss of lineage border integrity, in contrast to what has been reported in the *Twist*$^{+/-}$ mutants [17]. Coronal craniosynostosis in the mesoderm mutants occurs in the absence of a primary defect of the neural crest-derived dura mater underlying the coronal suture [16]. Finally, Holmes and Basilico showed that neural crest mutants are characterized by premature fusion of several facial sutures at P0 (i.e. frontal-premaxillary, maxillary-premaxillary, zygomatico-maxillary, and zygomatico-squamosal sutures) associated with medium to strong midfacial

hypoplasia as expected in the Apert syndrome phenotype, and retroflexion of the cranial base.

Mesodermal expression of the *Fgfr2*^{S252W} allele was associated with highly variable facial phenotypes, including specimens with extreme facial shortening, even though none of the facial skeletal sutures were reported to be prematurely fused at birth [16]. These observations imply that dysmorphogenesis of regions derived from the neural crest occur secondarily even when the expression of the mutation is limited to mesoderm-derived cells and tissues. However, the mechanisms that underlie these secondary effects are unknown. Comparable secondary effects of neural crest expression of the FGFR2 S252W mutation on mesoderm-derived bones were not reported [16].

Using micro computed tomography (μCT) images, we quantify craniofacial shape variation among Apert syndrome mouse models that express the FGFR2 S252W mutation exclusively in either mesoderm- or in neural crest-derived tissues and their unaffected littermates to identify patterns of craniofacial shape variation and craniofacial suture fusion. We pay particular attention to the dysmorphic regions derived from the lineage not expressing the mutation and define the shape changes in these regions as ‘secondary’ relative to the primary shape changes occurring in the tissues derived from the lineage expressing the mutation. Tissue-specific genetic models are helpful in more clearly identifying and quantifying such secondary shape changes which are difficult to characterize in full Apert mouse models where the mutation is ubiquitously expressed. We have previously shown that in the full FGFR2-related syndrome models, mutations thought primarily to affect cells of one type (e.g., osteoprogenitor) can have equally profound effects on cells that make up other tissues (e.g., brain, vitreous, skin) [18–21], thereby contributing to tissue-level behaviors of morphological development. Moreover, interaction among various skull components [22] is known to occur during growth such that dysmorphology specific to a skull region can have profound effects on other regions [23]. Our precise quantification of primary shape changes caused by mutation-driven alterations in cellular behavior and secondary shape changes caused by a conformational adjustment to the primary changes captures the overall pattern of shape changes specific to each group in our study.

Our objective is twofold: (i) to quantitatively define the anatomical locations that show morphological changes that are secondary to lineage-specific, localized expression of the FGFR2 S252W mutation; and (ii) to determine the relationship between suture fusion pattern and these secondary shape changes. We hypothesize that when the suture mesenchyme originates from the same cell lineage as the one expressing the FGFR2 S252W Apert syndrome mutation, the suture will be prematurely fused (H1). We also hypothesize that craniofacial shape of newborn (P0) mice expressing the FGFR2 S252W mutation in the neural crest-derived tissues will be more severely affected than in P0 mice expressing the mutation only in mesoderm-derived tissues because the majority of the bones and sutures constituting the skull at P0 are neural crest-derived (H2).

2 Materials and methods

2.1 Mice

Mice were bred using a Cre-inducible Apert syndrome mouse model [13,14] combined with either mesoderm- or neural crest specific Cre [11,12]. Mice were bred on a mixed background, and genotyped by PCR of genomic DNA prepared from tail-tips for *Fgfr2*, *Neo* and *Cre* as described [14,16]. All mice are heterozygous for a Cre. Mice carrying the Apert mutation are all heterozygous for the floxed *Fgfr2* S252W allele. Control mice are homozygous for the wild type *Fgfr2* allele. These mouse models have been described by Holmes and Basilico [16]. For clarity, $Mesp1Cre^{Tg/+}/\ Fgfr2^{+/S252WNeo}$ and $Mesp1Cre^{Tg/+}/\ Fgfr2^{+/+}$ mice are referred to as $Meso^{+/S252W}$ and $Meso^{+/+}$, respectively. Likewise, $Wnt1Cre^{Tg/+}/\ Fgfr2^{+/S252WNeo}$ and $Wnt1Cre^{Tg/+}/\ Fgfr2^{+/+}$ mice are referred to as $NC^{+/S252W}$ and $NC^{+/+}$, respectively.

2.2 Images

μCT images of the skulls of $Meso^{+/S252W}$ (n=22), $Meso^{+/+}$ (n=20), $NC^{+/S252W}$ (n=15), and $NC^{+/+}$ (n=19) mice were acquired by the HD-600 OMNI-X scanner (Bio-Imaging Research Inc, Lincolnshire, IL; 100kV, 0.19mA) at the Center for Quantitative X-Ray Imaging, Pennsylvania State University (www.cqi.psu.edu) with a pixel size of 0.0135 × 0.0135mm and a slice thickness of 0.0156mm. Image data were reconstructed on a 1024 × 1024 pixel grid as 16 bit TIFF and subsequently reduced to 8 bit TIFF for image analysis. Bone was segmented using solid hydroxyapatite phantoms (QRM GmbH, Möhrendorf, Germany) imaged with the specimens allowing us to linearly associate relative x-ray attenuation values with bone mineral density estimates.

2.3 Cranial sutures

Patency of cranial sutures was scored on 3D skull reconstructions of all 76 mice. Four stages were defined: (i) patent (P), the suture remains open and no bridges or partial fusion is observed; (ii) bridging (B), bone bridging the two bones separated by the suture is detected, but bridges remain few and thin; (iii) partially fused (PF), the suture is fused, but only to a maximum of approximately 75% of its length; (iv) fused (F): more than 75% of the suture is fused.

Because of the small degree of asymmetry in the suture fusion pattern of the right and left sides of a same bilateral suture (Fig. S1), patency stages for bilateral sutures were re-coded into a single variable representing the average state of suture patency by computing the sample mean between the left and right sides of mice displaying the same stage of suture fusion (e.g., 10 mice with the left side of the coronal suture fused and 8 mice with the right side of the coronal suture fused is coded as 9 mice with the coronal suture fused).

2.4 Histology and histochemistry

LacZ activity was detected as previously described [24]. For lacZ staining of sections, embryonic day (E) 16.5 heads were skinned and fixed in glutarate/formaldehyde buffer for 1.5–2h at 4°C, washed in PBS, equilibrated in 30% sucrose/PBS, then embedded in Tissue-Tek OTC Compound (Sakura, Japan). Frozen sections of 10 μm thickness were cut on a

Microm Cryostat and transferred to Superfrost Plus microscope slides (Fisher Scientific, USA). Counterstaining was done with Eosin Y (E4382, Sigma, USA).

2.5 Landmark data collection and analysis

3D reconstructions of the skulls from μCT images were based on information from solid hydroxyapatite phantoms. Sixty-seven 3D landmark coordinates were digitized on the surfaces of reconstructed skulls in Avizo 6 (Visualization Sciences Group, VSG) (Table S1 and fig. S2).

To extract shape information defined on the basis of the landmarks, we performed Generalized Procrustes analysis, a procedure that translates, rotates and scales configurations of landmarks until a best fit of corresponding landmarks is achieved [25,26]. The resulting coordinates (Procrustes coordinates) permit the computation of a coordinate-wise average shape, the Procrustes average shape (PAS) [27]. The PAS triangular mesh can be obtained by warping the triangular mesh of one mouse to the landmark set corresponding to the PAS. Procrustes shape coordinates are analyzed by principal components analysis (PCA) [28]. The principal components contain the loadings for the linear combinations of the original variables and can be visualized as shape deformation illustrated by wireframes (Fig. S1). To facilitate visualization of shape differences between two consensus shapes (for example the PAS of the *Meso*$^{+/S252W}$ mice and that of the *NC*$^{+/S252W}$ mice), we present a color map produced by comparing the corresponding surface warps. The color map has been computed in Avizo 6 (Visualization Sciences Group, VSG) and corresponds to the vector field computed by the difference of the vertex positions of corresponding vertices in both PAS surface warps.

3 Results

3.1 NC$^{+/S252W}$ mutant mice display the most distinctive suture fusion pattern

Figure 1 illustrates suture fusion patterns for the four groups of mice. Non-mutant mice display similar suture fusion patterns, though suture fusion in the *Meso*$^{+/+}$ mice appears slightly more advanced relative to the *NC*$^{+/+}$ mice. *Meso*$^{+/S252W}$ mutants mainly differ from non-mutant mice in the frontal-parietal (i.e. coronal), parietal-squamosal, frontal-maxillary, and vomer-maxillary suture fusion pattern. The coronal suture is almost systematically fused in the *Meso*$^{+/S252W}$ mice while the parietal-squamosal and vomer-maxillary sutures are more often patent. About 80% of the *Meso*$^{+/S252W}$ mice display a patent frontal-maxillary suture, while this suture is patent for 100% of the non-mutant mice.

The *NC*$^{+/S252W}$ mice show multiple partial or fully prematurely fused sutures including the premaxillary-maxillary, maxillary-palatine, palatine-alisphenoid, maxillary-zygomatic, and frontal-maxillary sutures. Fusion of the zygomatic-squamosal, frontal-squamosal, parietal-squamosal, frontal-nasal, and vomer-premaxillary sutures is also relatively more advanced in *NC*$^{+/S252W}$ mutants. Conversely, the para- and mid-sagittal sutures (e.g., inter-premaxillary, inter-palatine, vomer-maxillary, palatine-presphenoid sutures) are less often fused or partially fused in *NC*$^{+/S252W}$ mutants relative to the other three groups. The mutant groups share similar degrees of patency for the inter-maxillary, inter-nasal, and palatine-basisphenoid sutures. Finally, at P0 all four groups of mice display patent inter-parietal

(sagittal), inter-frontal (metopic), frontal-alisphenoid, frontal-nasal, and frontal-premaxillary sutures (not shown).

Coronal sections of the inter-premaxillary, inter-maxillary, and inter-palatine sutures all stain for Xgal in E16.5 Wnt1-Cre/R26R mice confirming the neural crest origin of the mesenchyme of these sutures (Figs. 2, panels A–D). These sutures, and all the surrounding tissues, are negative for staining in E16.5 Mesp1-Cre/R26R mice (Figs. 2, panels A′–D′).

These results on suture fusion pattern lead us to reject hypothesis H1, which proposed that premature suture fusion will occur in those sutures where the mesenchyme originates from the same lineage as that expressing the FGFR2 S252W Apert syndrome mutation. Indeed, we demonstrate that in the $NC^{+/S252W}$ mutants the rostral part of the inter-parietal (sagittal) suture, along with the inter-frontal (metopic), inter-nasal, inter-premaxillary, inter-maxillary, and inter-palatine sutures, all neural crest-derived [1], remain patent at P0. Assuming a neural crest origin in mice for the abnormally patent vomer-maxillary, and palatine-presphenoid sutures adds to the lack of support for H1.

3.2 $NC^{+/S252W}$ mutant mice primary shape changes mainly involve the snout, rostral neurocranial, and rostral cranial base regions

Since the facial skeleton, the frontal and squamosal components of the cranial vault, and the rostral aspect of the cranial base are neural crest-derived (Fig. 3, panel A), we expect $NC^{+/S252W}$ mutants to display primary dysmorphologies in these regions (Figs. 3, panels B and C). We used principal components analysis to examine the overall cranial variation in our sample. The first principal component (PC1) accounts for 28.5% of the total variance in the sample and clearly separates the $NC^{+/S252W}$ mutants from the $Meso^{+/S252W}$, $Meso^{+/+}$, and $NC^{+/+}$ mice (Fig. 3, panel D). As expected, shape changes associated with PC1 mainly involve neural crest-derived bones, and $NC^{+/S252W}$ mutants corresponding to the negative scores on PC1 display primary dysmorphologies in aspects of the snout, cranial base and cranial vault. The direct comparison of cranial shape between the $NC^{+/S252W}$ and $NC^{+/+}$ in a separate analysis results in shape differences similar to those described between these two groups by PC1 in figure 3 (results not shown). The $Meso^{+/S252W}$ mice overlap with the unaffected mice on PC1 implying that shape variation in these anatomical regions is normal for these mice and not related to the expression of the mutation in the neural crest derived-tissues. Compared to the $Meso^{+/S252W}$, $Meso^{+/+}$, and $NC^{+/+}$ mice, the $NC^{+/S252W}$ mice display a wider and (dorso-ventrally) expanded cranial vault, a retracted snout, and retroflexion of the cranial base (Figs. 3, panels B, C and E). Most of the sutures that connect the maxilla with surrounding bones are fused (except for the maxillary-nasal and vomer-maxillary sutures) and the maxillary region is contracted rostrocaudally and wider compared to the other groups of mice. The zygomatic-maxillary suture is prematurely fused and the zygomatic bone is displaced ventrally. The premaxillae, which are wider and retracted, though not reduced rostrocaudally, are associated with an abnormally patent inter-premaxillary suture, and prematurely fused maxillary-premaxillary and vomer-premaxillary sutures. The more ventrally placed palatine bones are associated with a prematurely fused palatine-maxillary suture and delayed fusion of inter-palatine and palatine-presphenoid sutures. The more dorsally placed vomer and presphenoid together with the more ventrally

placed basisphenoid describe retroflexion of the cranial base (Figs. 3 panels C and E). Finally, the frontal bones are placed more dorsally and more laterally, forming a large gap between them. The prematurely fused frontal-maxillary suture is associated with a more lateral placement of the most caudal aspect of the frontal bones compared to the most rostral aspect.

3.3 $NC^{+/S252W}$ mutant mice secondary shape changes occur in the basioccipital and parietal regions

We observed secondary shape changes in the mesoderm-derived bones of $NC^{+/S252W}$ mutants, particularly in the parietal and basioccipital regions (Figs. 4, panels A and D). Compared to the other groups of mice, the parietal bones of the $NC^{+/S252W}$ mutants are higher and shifted laterally. The non-mutant parietal bones and the mutant frontal bones are delimited by a non-mutant coronal suture which is patent and presumed to preserve a normal growth potential. The rostrocaudally elongated basioccipital is placed more ventrally and is connected to the basisphenoid through a patent and apparently functioning spheno-occipital synchondrosis, a cartilaginous joint of dual origin [2]. Neither the lateral occipital nor the supraoccipital display shape differences when compared to unaffected mice (Figs. 4, panels A and D).

3.4 $Meso^{+/S252W}$ mutant mice primary shape changes are in the parietal regions

The second principal component (21.9%) separates the $Meso^{+/S252W}$ mutants from the $NC^{+/S252W}$, $NC^{+/+}$, and $Meso^{+/+}$ mice (Fig. 3, panel D). The shape changes associated with PC2 involve mesoderm- and neural crest-derived bones. The primary shape changes on PC2 show the $Meso^{+/S252W}$ mutants to have a more rostrally shifted parietal region, a rostrocaudally enlarged posterior aspect of the basioccipital, and a more dorsally placed supraoccipital compared to the other groups (Fig. 3, panel E and fig. 4, panel D). The direct comparison of cranial shape between the $Meso^{+/S252W}$ and $Meso^{+/+}$ in a separate analysis results in shape differences similar to those described between these two groups by PC2 in figure 3 (results not shown). The $NC^{+/S252W}$ mice show considerable within-group variation and overlap with the unaffected mice on PC2 implying that shape variation accounted for by negative values on PC2 is like that of unaffected mice and not related to the expression of the mutation in the mesoderm derived-tissues. The only characteristic suture fusion patterns are the prematurely fused coronal suture (i.e. frontal-parietal) and the abnormally patent parietal-squamosal suture (Fig. 1).

3.5 $Meso^{+/S252W}$ mutant mice secondary shape changes are in the frontal and snout regions

The majority of the dysmorphic cranial regions in $Meso^{+/S252W}$ mutants occur in neural crest-derived regions. Secondary shape changes characterizing the P0 $Meso^{+/S252W}$ mutants when compared to the other mice include a more dorsally deflected snout relative to the palate, and ventrally placed basisphenoid, and palatal bones (Fig. 4, panels B and D). None of these bones have neighboring sutures that are prematurely fused and the vomer-maxillary suture is abnormally patent (Fig. 1). This implies that the growth potential of the non-mutant facial sutures is conserved, supported by the fact that these bones are not rostrocaudally

contracted. The relative position of the frontal bone is driven by the primary shape changes and anterior placement of the parietal bones.

3.6 Skull dysmorphology of $NC^{+/S252W}$ mutants is increased relative to $Meso^{+/S252W}$ mutants

We further compared the consensus shapes (PAS) of the $Meso^{+/S252W}$ and $NC^{+/S252W}$ mutants to illustrate specific shape differences between these two groups (Fig. 4). The most intense shape differences between the $Meso^{+/S252W}$ and $NC^{+/S252W}$ mutants are in the frontal, parietal, squamous temporal, premaxilla, and presphenoid regions (Figs. 4, Panels C and D). The $NC^{+/S252W}$ mutants display a more doming cranial vault, the region where the frontal bones articulate with the nasal bones is steeper than the $Meso^{+/S252W}$, the rostral aspect of the premaxilla is contracted and more ventrally placed, and the zygomatic bones and the zygomatic processes of both squamous temporal and maxilla are dorsally placed. The frontal, parietal, squamous temporal, premaxilla, and most of the maxilla regions are all extended laterally making the skull of the $NC^{+/S252W}$mice wider than that of the $Meso^{+/S252W}$ mice. These observations coupled with the distribution of the four groups of mice in the shape space (Fig. 3, panel D) and the suture fusion pattern support H2 proposing that $NC^{+/S252W}$ mutants have a more dysmorphic skull than the $Meso^{+/S252W}$ mutants.

4 Discussion

We have used mouse models expressing the FGFR2 S252W mutation either in mesoderm- or neural crest-derived tissues [16] to quantify differences in craniofacial shape variation and suture fusion patterns and to identify shape changes in craniofacial bones derived from the lineage not expressing the mutation, referred to here as secondary shape changes. Our results lead to a strong rejection of H1 proposing that when the suture mesenchyme originates from the same lineage as the one expressing the FGFR2 S252W mutation, the suture will be fused prematurely, but fully support H2 proposing that at birth, $NC^{+/S252W}$ mutants are more severely affected than $Meso^{+/S252W}$ mutants.

The recent report by Lewis et al. [29] that Wnt1-Cre transgenic mice exhibit phenotypes in multiple aspects of midbrain development confirms results reported by Danielian et al. [11] and potentially complicate the utility of this mouse model in studies like as ours. To address this problem we directly compared the cranial phenotypes of $NC^{+/+}$ and $Meso^{+/+}$ mice in a separate analysis (Fig. S3) revealing similarity in cranial shape for these two groups. These results indicate that the midbrain dysmorphologies caused by ectopic expression of *Wnt1* in $NC^{+/+}$ mice do not cause cranial shape changes at P0.

The skull shape of $NC^{+/S252W}$ mutants is characterized by a retracted snout, a doming cranial vault and retroflexion of the cranial base (Fig. 3). As expected, these dysmorphic features mainly involve neural crest-derived bones. Secondary shape changes in $NC^{+/S252W}$ mutants are the most intense for the mesoderm-derived parietal and basioccipital bones (Fig. 3). It has been shown that proliferation of the non-mutant parietal osteogenic front adjacent to the coronal suture was unaffected at E16.5, while proliferation of the mutant frontal was decreased significantly (67% of the non-mutant frontal rate) in $NC^{+/S252W}$ mutants [16]. We interpret the abnormal placement of the parietal bones as the consequence of the prematurely

fused frontal-maxillary suture associated with the relatively preserved growth potential of the coronal suture resulting in the characteristic domed cranial vault of the $NC^{+/S252W}$ mutants. We interpret the characteristic position of the basioccipital in $NC^{+/S252W}$ mutants as the consequence of the ventral placement of the basisphenoid and palatine bones. Additionally, we cannot totally exclude the potential influence of the brain on the secondary shape changes recorded in $NC^{+/S252W}$ mutants since the brain and skull maintain an intimate relationship throughout development [30]. It has been shown that *Wnt1* is also expressed in the caudal diencephalon, dorsal and ventral midlines of the midbrain, and midbrain-hindbrain junction where the possibility of ectopic *Wnt1* activity acting synergistically with the FGFR2 S252W mutation could exist [11]. However, determining the specific role of brain development in the production of skull shape in mutant and non-mutant mice would require specific measures of brain morphology and neural cellular dynamics not available from our μCT data.

The skull shape of $Meso^{+/S252W}$ mutants is characterized by a more dorsally deflected snout relative to the palate, ventrally placed basisphenoid and basioccipital, and a rostrally shifted frontal and parietal region (Fig. 3). The dysmorphic features of the $Meso^{+/S252W}$ mutants were not limited to the mesoderm-derived bones but instead primarily involved neural crest-derived bones (e.g., snout). It has been shown that proliferation in both the mutant parietal and non-mutant frontal osteogenic fronts were decreased at E16.5 (approximately 35% of the non-mutant frontal and parietal rates) [16]. We interpret the premature fusion of the coronal suture and the associated reduction of the frontal proliferation as being the main factor responsible for the dorsally deflected snout.

The amount of craniofacial phenotypic variation as recorded by the PCA (Fig. 3, panel D), particularly by PC2, is larger for the two mutant groups than for the unaffected mice. This result corroborates previous reports of increased variation in mouse models carrying genetic orthologues of human conditions relative to unaffected littermates [31–34]. Additionally, it could be argued that the mixed background used in these experiments more closely resembles the human condition (relative to an inbred background), providing an appropriate analogue for the phenotypic outcome associated with the mutation.

4.1 Fusion pattern of the sagittal oriented sutures in $NC^{+/S252W}$ mutants demonstrate that expression of the FGFR2 S252W mutation in the suture mesenchyme is not sufficient to induce premature fusion

The absence of premature fusion of the neural crest-derived sagittal, metopic, inter-nasal, inter-premaxillary, inter-maxillary, and inter-palatine sutures in $NC^{+/S252W}$ mutants at P0 [1] supports the premise that premature fusion of a suture does not exclusively depend on the expression of the FGFR2 S252W mutation in the sutural mesenchyme. More support for this finding is provided if we assume neural crest origin for the vomer-maxillary and palatine-presphenoid sutures, which remained abnormally patent in $NC^{+/S252W}$ mutants when compared to the other mice (Fig. 1). In Apert syndrome, the sagittal and metopic sutures fail to develop properly, and instead bony islands form within a wide midline defect and large anterior fontanelle that eventually fill with bone during the first two years of life, in a process called sutural agenesis [6]. Wang et al. [35] also described a wide gap between the

frontal bones in the full *Fgfr2*$^{+/S252W}$ mutants. The neural crest-derived sutures of the *NC*$^{+/S252W}$ mutants show similar results as those recently reported on the fusion pattern of facial sutures in *Fgfr2*$^{+/S252W}$ mutants, while these sutures in *Meso*$^{+/S252W}$ mutants show similar fusion pattern as that reported for unaffected mice [36,37].

All of these neural crest-derived sutures that remain abnormally patent in Apert syndrome and in newborn *NC*$^{+/S252W}$ and *Fgfr2*$^{+/S252W}$ mutants are located on para- or mid-sagittal planes. Is there a fundamental difference in suture biogenesis or signaling in the sutures that form on the sagittal plane? Or is the difference based on relative timing of suture closure; the sutures in the sagittal plane being delayed in their fusion pattern secondarily to compensate the abnormal fusion of transversal sutures taking place earlier? Equivocal findings are reported on that issue. Komatsu et al. [38] reported that enhanced bone morphogenetic protein (BMP) in cranial neural crest cells and derived pre-osteoblasts causes premature fusion of the rostral part of the metopic suture contrary to the augmentation of FGF-ERK1/2 signaling which does not cause synostosis. Their study is in agreement with a recent genome-wide association study which identified susceptibility loci for nonsyndromic sagittal craniosynostosis near BMP2 [39]. Martínez-Abadías et al. [37] reported abnormal patterns of proliferation, differentiation, and apoptosis in the inter-premaxillary suture of *Fgfr2*$^{+/S252W}$ mutants resulting in abnormal patency of this suture at P0. Together, these observations suggest biogenesis differences in cranial sutures that form on the sagittal plane relative to transverse sutures. However, report of the inter-palatine suture being occasionally partially fused in 3-week old *NC*$^{+/S252W}$ mutants [16] and the unaffected patterns of proliferation, differentiation, and apoptosis associated with an abnormally patent condition at P0 [37] seem to favor, at least for this suture, a timing issue.

4.2 Retroflexion of the cranial base is only evident in NC$^{+/S252W}$ mutants

Contrary to what was previously reported for these mice using histological sections [16], our results show that the *NC*$^{+/S252W}$ mutants display retroflexion of the cranial base at P0, while the orientation of the cranial base of the *Meso*$^{+/S252W}$ mutants is not different from non-mutant mice (Figs. 3, panels C and E). μCT images of all mice and the ability to section the imaged skulls at any angle provided a clear way to evaluate cranial base dysmorphology in every individual. The most dysmorphic region of the cranial base in *NC*$^{+/S252W}$ mutants is local to the presphenoid and vomer, both of which are associated with neighboring sutures displaying abnormal fusion patterns, either prematurely fused (e.g., vomer-premaxillary) or abnormally patent (e.g., palatine-presphenoid and vomer-maxillary sutures).

Contrary to sutures of the cranial vault and the facial skeleton, the synchondroses of the cranial base (intra-occipital, spheno-occipital, inter-sphenoidal) are never prematurely fused at P0 in our samples confirming previous reports [36]. However, premature fusion of these basicranial joints may occur later in postnatal life as shown in one-year old *Meso*$^{+/S252W}$ mutants where the inter-sphenoidal synchondrosis was partially fused [16] and in older Apert syndrome patients where premature fusion of the spheno-ocipital synchondrosis has been reported [40].

5 Conclusions

Our results lead to two major conclusions. First, premature fusion of a suture is not necessarily dependent on the expression of the FGFR2 S252W mutation in the sutural mesenchyme. It appears that suture fusion patterns in both mouse models are suture-specific resulting from a complex combination of the influence of primary abnormalities of biogenesis or signaling in the sutures, and variation in individual timing specific to each suture. Second, we identified shape changes in regions of the skull derived from the lineage that did not express the mutation (i.e. the secondary shape changes). Though our study has focused on the effects of the conditional expression of the FGFR2 S252W mutation on developing bone, we realize that in the $NC^{+/S252W}$ and $Meso^{+/S252W}$ mutants this mutation is also expressed in soft tissues causing primary changes that could also contribute to the secondary skeletal anomalies quantified here.

We propose that the secondary changes that we identified in the skull derive from four potential sources: (i) disrupted morphogenesis of the non-mutant bone caused by a neighboring synostosed suture resulting in abnormal shape; (ii) displacement of the non-mutant bone caused by neighboring dysmorphic mutant bones articulating with the non-mutant bone through functioning sutures or synchondroses; (iii) functional pressures of soft tissues whose morphology and growth dynamics are affected by these mutations; and (iv) communication of cell signaling or soluble factors produced by mutant cells that alter the development of the neighboring non-mutant cells. Specific research designs are required to determine the relative role of these potential processes in the production of craniofacial dysmorphogenesis in craniosynostosis conditions.

Supplementary Material

Refer to Web version on PubMed Central for supplementary material.

Acknowledgments

We are grateful to Dr. Christopher Percival for discussion on a previous version of this manuscript, and to Dr. Susan Motch, Tiffany Kim, and Hongseok Kim for managing the mice for imaging and the related image data. This work was supported by the National Institute of Dental and Craniofacial Research (Grant Numbers R01DE018500 and R01DE022988), the National Institute of Arthritis and Musculoskeletal and Skin Diseases (Grant Number AR051358), and the National Institute of Child Health and Development (R01-HD038384).

Abbreviations

as	alisphenoid
bo	basioccipital
bs	basisphenoid
FGFR2	fibroblast growth factor receptor 2
***Fgfr2*$^{+/S252W}$**	ubiquitous *Fgfr2* S252W mutants
fr	frontal

μCT	high resolution computed tomography
ipa	interparietal
la	lacrimal
lo	lateral occipital
***Meso*$^{+/+}$**	*Mesp1Cre*$^{Tg/+}$/ *Fgfr2*$^{+/+}$
***Meso*$^{+/S252W}$**	*Mesp1Cre*$^{Tg/+}$/ *Fgfr2*$^{+/S252WNeo}$
mx	maxilla
na	nasal
***NC*$^{+/+}$**	*Wnt1Cre*$^{Tg/+}$/ *Fgfr2*$^{+/+}$
***NC*$^{+/S252W}$**	*Wnt1Cre*$^{Tg/+}$/ *Fgfr2*$^{+/S252WNeo}$
P0	postnatal day 0 (newborn)
pa	parietal
pal	palatine
pmx	premaxilla
PC	principal component
PCA	principal components analysis
so	supraoccipital
sqm	squamosal
vom	vomer
zyg	zygomatic

References

1. Jiang X, Iseki S, Maxson RE, Sucov HM, Morriss-Kay GM. Tissue origins and interactions in the mammalian skull vault. Dev Biol. 2002; 241:106–16. [PubMed: 11784098]
2. McBratney-Owen B, Iseki S, Bamforth SD, Olsen BR, Morriss-Kay GM. Development and tissue origins of the mammalian cranial base. Dev Biol. 2008; 322:121–32. [PubMed: 18680740]
3. Yoshida T, Vivatbutsiri P, Morriss-Kay G, Saga Y, Iseki S. Cell lineage in mammalian craniofacial mesenchyme. Mech Dev. 2008; 125:797–808. [PubMed: 18617001]
4. Opperman LA. Cranial sutures as intramembranous bone growth sites. Dev Dyn. 2000; 219:472–85. [PubMed: 11084647]
5. Johnson D, Wilkie AOM. Craniosynostosis. Eur J Hum Genet. 2011; 19:369–76. [PubMed: 21248745]
6. Cohen, MM.; MacLean, RE. Craniosynostosis: Diagnosis, Evaluation, and Management. 2. Oxford University Press; USA: 2000.
7. Cohen MM Jr, Kreiborg S, Lammer EJ, Cordero JF, Mastroiacovo P, Erickson JD, et al. Birth prevalence study of the Apert syndrome. Am J Med Genet. 1992; 42:655–9. [PubMed: 1303629]
8. Wilkie AO, Slaney SF, Oldridge M, Poole MD, Ashworth GJ, Hockley AD, et al. Apert syndrome results from localized mutations of FGFR2 and is allelic with Crouzon syndrome. Nat Genet. 1995; 9:165–72. [PubMed: 7719344]

9. Allanson JE, Cunniff C, Hoyme HE, McGaughran J, Muenke M, Neri G. Elements of Morphology: Standard Terminology for the Head and Face. Am J Med Genet A. 2009; 149A:6–28. [PubMed: 19125436]
10. Cunningham ML, Seto ML, Ratisoontorn C, Heike CL, Hing AV. Syndromic craniosynostosis: from history to hydrogen bonds. Orthod Craniofac Res. 2007; 10:67–81. [PubMed: 17552943]
11. Danielian PS, Muccino D, Rowitch DH, Michael SK, McMahon AP. Modification of gene activity in mouse embryos in utero by a tamoxifen-inducible form of Cre recombinase. Curr Biol. 1998; 8:1323–6. [PubMed: 9843687]
12. Saga Y, Miyagawa-Tomita S, Takagi A, Kitajima S, Miyazaki Ji, Inoue T. MesP1 is expressed in the heart precursor cells and required for the formation of a single heart tube. Development. 1999; 126:3437–47. [PubMed: 10393122]
13. Chen L, Li D, Li C, Engel A, Deng C-X. A Ser252Trp [corrected] substitution in mouse fibroblast growth factor receptor 2 (Fgfr2) results in craniosynostosis. Bone. 2003; 33:169–78. [PubMed: 14499350]
14. Holmes G, Rothschild G, Roy UB, Deng C-X, Mansukhani A, Basilico C. Early onset of craniosynostosis in an Apert mouse model reveals critical features of this pathology. Dev Biol. 2009; 328:273–84. [PubMed: 19389359]
15. Soriano P. Generalized lacZ expression with the ROSA26 Cre reporter strain. Nat Genet. 1999; 21:70–1. [PubMed: 9916792]
16. Holmes G, Basilico C. Mesodermal expression of Fgfr2S252W is necessary and sufficient to induce craniosynostosis in a mouse model of Apert syndrome. Dev Biol. 2012; 368:283–93. [PubMed: 22664175]
17. Merrill AE, Bochukova EG, Brugger SM, Ishii M, Pilz DT, Wall SA, et al. Cell mixing at a neural crest-mesoderm boundary and deficient ephrin-Eph signaling in the pathogenesis of craniosynostosis. Hum Mol Genet. 2006; 15:1319–28. [PubMed: 16540516]
18. Aldridge K, Hill CA, Austin JR, Percival C, Martinez-Abadias N, Neuberger T, et al. Brain phenotypes in two FGFR2 mouse models for Apert syndrome. Dev Dyn. 2010; 239:987–97. [PubMed: 20077479]
19. Percival CJ, Wang Y, Zhou X, Jabs EW, Richtsmeier JT. The effect of a Beare-Stevenson syndrome Fgfr2 Y394C mutation on early craniofacial bone volume and relative bone mineral density in mice. J Anat. 2012; 221:434–42. [PubMed: 22881429]
20. Wang Y, Zhou X, Oberoi K, Phelps R, Couwenhoven R, Sun M, et al. p38 Inhibition ameliorates skin and skull abnormalities in Fgfr2 Beare-Stevenson mice. J Clin Invest. 2012; 122:2153–64. [PubMed: 22585574]
21. Martínez-Abadías N, Motch SM, Pankratz TL, Wang Y, Aldridge K, Jabs EW, et al. Tissue-specific responses to aberrant FGF signaling in complex head phenotypes. Dev Dyn. 2013; 242:80–94. [PubMed: 23172727]
22. Moss ML, Young RW. A functional approach to craniology. Am J Phys Anthropol. 1960; 18:281–92. [PubMed: 13773136]
23. Olson, EC.; Miller, RL. Morphological Integration. 1. University Of Chicago Press; 1958.
24. Sanes JR, Rubenstein JL, Nicolas JF. Use of a recombinant retrovirus to study post-implantation cell lineage in mouse embryos. EMBO J. 1986; 5:3133–42. [PubMed: 3102226]
25. Rohlf F, Slice D. Extensions of the Procrustes method for the optimal superimposition of landmarks. Syst Zool. 1990; 39:40–59.
26. Dryden, IL.; Mardia, KV. Statistical Shape Analysis. Chichester: Wiley; 1998.
27. Mitteroecker P, Gunz P. Advances in geometric morphometrics. Evol Biol. 2009; 36:235–47.
28. Jolliffe, IT. Principal component analysis. New York: Springer; 2002.
29. Lewis AE, Vasudevan HN, O'Neill AK, Soriano P, Bush JO. The widely used Wnt1-Cre transgene causes developmental phenotypes by ectopic activation of Wnt signaling. Dev Biol. 2013; 379:229–34. [PubMed: 23648512]
30. Richtsmeier JT, Flaherty K. Hand in glove: brain and skull in development and dysmorphogenesis. Acta Neuropathol. 2013; 125:469–89. [PubMed: 23525521]

31. Richtsmeier JT, Baxter LL, Reeves RH. Parallels of craniofacial maldevelopment in Down syndrome and Ts65Dn mice. Dev Dyn. 2000; 217:137–45. [PubMed: 10706138]
32. Hallgrímsson B, Willmore K, Hall BK. Canalization, developmental stability, and morphological integration in primate limbs. Am J Phys Anthropol. 2002; (Suppl 35):131–58. [PubMed: 12653311]
33. Willmore KE, Zelditch ML, Young N, Ah-Seng A, Lozanoff S, Hallgrímsson B. Canalization and developmental stability in the Brachyrrhine mouse. J Anat. 2006; 208:361–72. [PubMed: 16533318]
34. Parsons TE, Kristensen E, Hornung L, Diewert VM, Boyd SK, German RZ, et al. Phenotypic variability and craniofacial dysmorphology: increased shape variance in a mouse model for cleft lip. J Anat. 2008; 212:135–43. [PubMed: 18093101]
35. Wang Y, Xiao R, Yang F, Karim BO, Iacovelli AJ, Cai J, et al. Abnormalities in cartilage and bone development in the Apert syndrome FGFR2(+/S252W) mouse. Development. 2005; 132:3537–48. [PubMed: 15975938]
36. Purushothaman R, Cox TC, Maga AM, Cunningham ML. Facial suture synostosis of newborn Fgfr1(P250R/+) and Fgfr2(S252W/+) mouse models of Pfeiffer and Apert syndromes. Birt Defects Res A Clin Mol Teratol. 2011; 91:603–9.
37. Martínez-Abadías N, Holmes G, Pankratz T, Wang Y, Zhou X, Jabs EW, et al. From shape to cells: mouse models reveal mechanisms altering palate development in Apert syndrome. Dis Model Mech. 2013; 6:768–79. [PubMed: 23519026]
38. Komatsu Y, Yu PB, Kamiya N, Pan H, Fukuda T, Scott GJ, et al. Augmentation of Smad-dependent BMP signaling in neural crest cells causes craniosynostosis in mice. J Bone Miner Res. 2013; 28:1422–33. [PubMed: 23281127]
39. Justice CM, Yagnik G, Kim Y, Peter I, Jabs EW, Erazo M, et al. A genome-wide association study identifies susceptibility loci for nonsyndromic sagittal craniosynostosis near BMP2 and within BBS9. Nat Genet. 2012; 44:1360–4. [PubMed: 23160099]
40. McGrath J, Gerety PA, Derderian CA, Steinbacher DM, Vossough A, Bartlett SP, et al. Differential closure of the spheno-occipital synchondrosis in syndromic craniosynostosis. Plast Reconstr Surg. 2012; 130:681e–689e. [PubMed: 22575855]

Highlights

- Neural crest-derived cranial bones are more severely affected by the FGFR2 S252W mutation than mesoderm-derived bones in newborn mice
- Cranial bones not derived from the lineage expressing the FGFR2 S252W mutation (either neural crest or mesoderm) also display dysmorphologies
- The FGFR2 S252W mutation affects fusion patterns differently in midline and transversal sutures

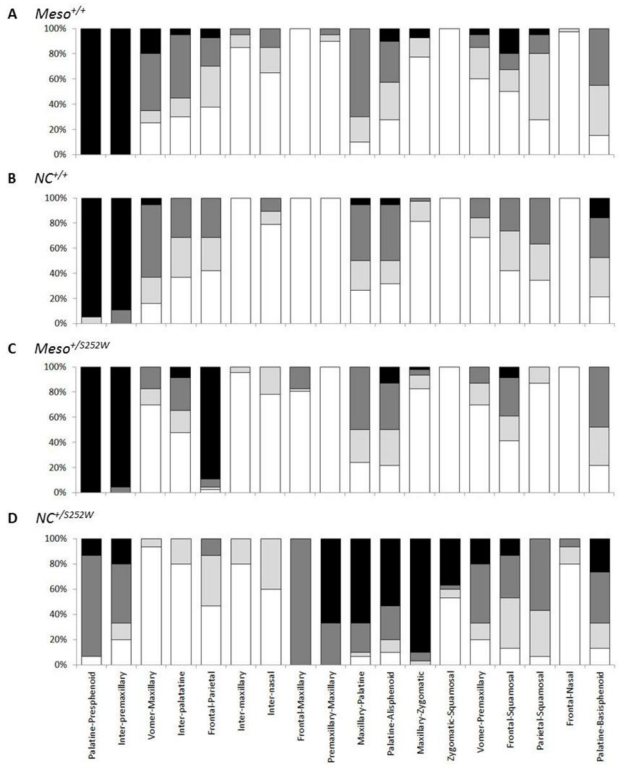

Fig. 1.

Suture fusion pattern in four groups of mice. Four stages were defined: patent (white); bridging (light grey); partially fused (dark grey); fused (black) (for the stages definition see Materials and methods section)

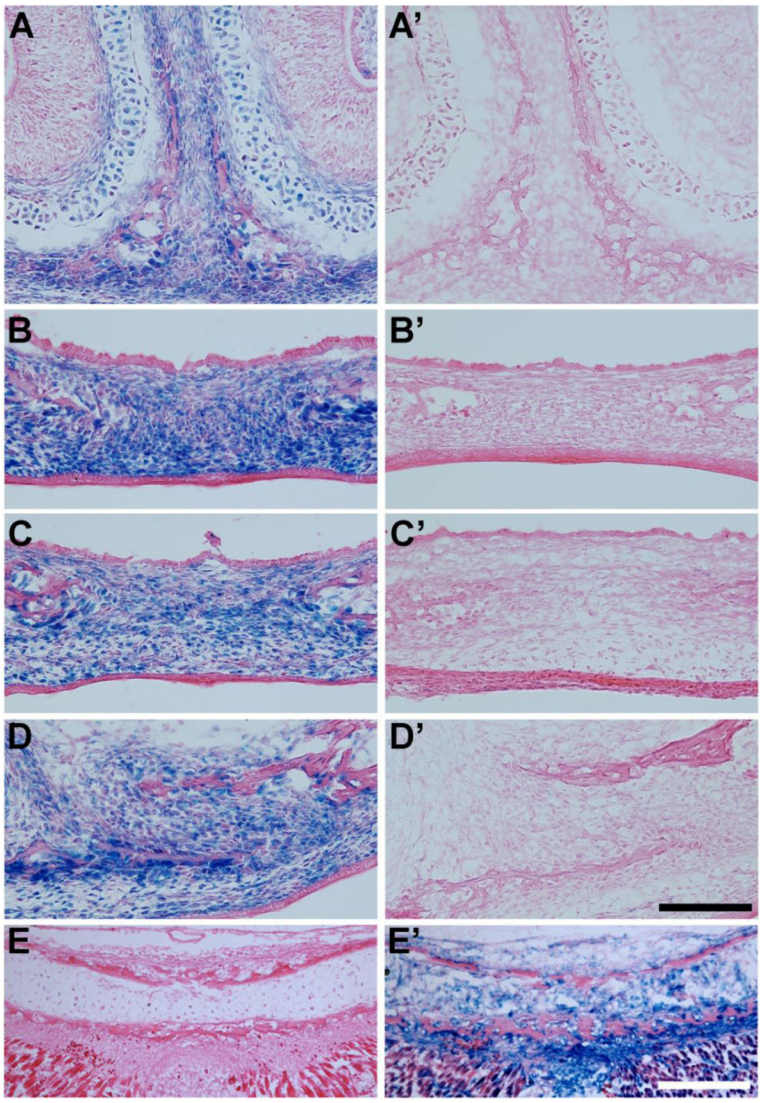

Fig. 2.

Facial sutures are derived from neural crest. The heads of E16.5 Wnt1-Cre/R26R (A–E) or Mesp1-Cre/R26R (A′–E′) were coronally sectioned and stained for β-galactosidase activity (blue). Sutures shown are (A, A′) Inter-premaxillary; (B, B′) Inter-maxillary; (C, C′) Inter-palatine; and (D, D′) Maxillary-Palatine. (E, E′) Sections through the mesoderm-derived basioccipital bone at the posterior of each head is shown. Slides are counter-stained with eosin (pink). Scale bars = 100 μm (A–D) and 200 μm (E, E′).

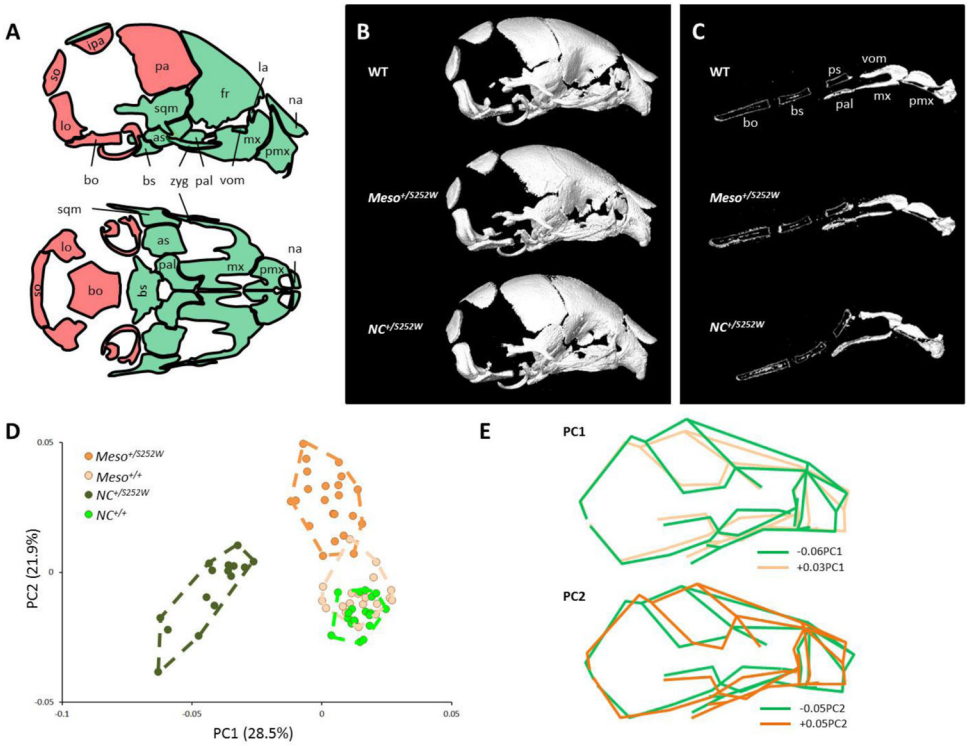

Fig. 3.

Skull shape differences between *Meso*$^{+/S252W}$ and *NC*$^{+/S252W}$ mutants and unaffected mice. Cellular origin of the skull at P0 is shown in lateral and ventral views in panel A (mesoderm-derived bones in pink, neural crest-derived bones in green) [1,2]. Lateral views of a wild type mouse, *Meso*$^{+/S252W}$ mutant (note the fused coronal suture), and NC$^{+/S252W}$ mutant from µCT reconstruction (panel B). Midsagittal section of the cranial base of a wild type mouse, *Meso*$^{+/S252W}$ mutant, and *NC*$^{+/S252W}$ mutant (note the retroflexion of the cranial base and vomer) from µCT reconstruction (panel C). Placement of the 77 *Meso*$^{+/S252W}$, *Meso*$^{+/+}$, *NC*$^{+/S252W}$, and *NC*$^{+/+}$ P0 mice on PC1 and PC2 in the skull shape space (principal component analysis of the landmarks Procrustes shape coordinates) (panel D). Shape changes visualized by wireframes associated with negative and positive scores on PC1 and PC2 (panel E).

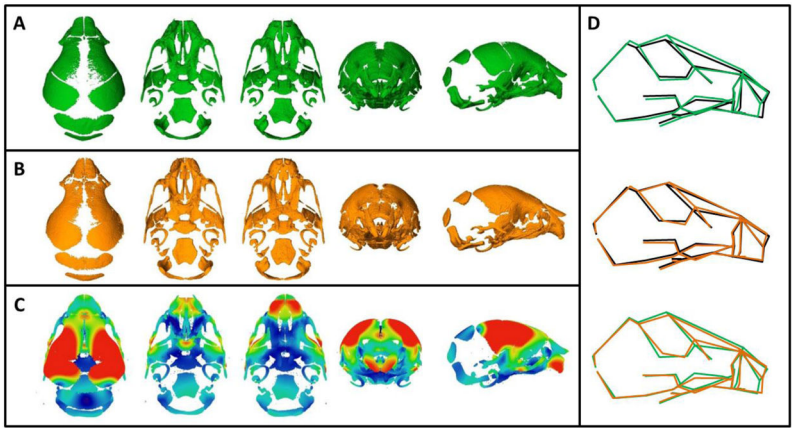

Fig. 4.

Comparison of the consensus shapes (PAS) of the $NC^{+/S252W}$ and $Meso^{+/S252W}$ mutants. Superior (with base removed), superior (with vault removed), inferior (with vault removed), anterior, and lateral views (reading from left to right) of the PAS of the $NC^{+/S252W}$ (panel A) and $Meso^{+/S252W}$ mutants (panel B). Color map representing the anatomical regions displaying the most and least intense shape differences (in red and dark blue respectively) between the $NC^{+/S252W}$ and $Meso^{+/S252W}$ mutants (panel C). Wireframes corresponding to the $NC^{+/S252W}$ (green) and $Meso^{+/S252W}$ (orange) mutants in lateral view when compared to the consensus shape of the unaffected mice (black) and to each other (panel D).